

NJC

Accepted Manuscript



This is an *Accepted Manuscript*, which has been through the Royal Society of Chemistry peer review process and has been accepted for publication.

Accepted Manuscripts are published online shortly after acceptance, before technical editing, formatting and proof reading. Using this free service, authors can make their results available to the community, in citable form, before we publish the edited article. We will replace this *Accepted Manuscript* with the edited and formatted *Advance Article* as soon as it is available.

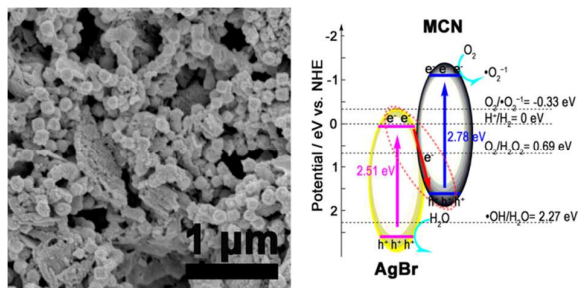
You can find more information about *Accepted Manuscripts* in the [Information for Authors](#).

Please note that technical editing may introduce minor changes to the text and/or graphics, which may alter content. The journal's standard [Terms & Conditions](#) and the [Ethical guidelines](#) still apply. In no event shall the Royal Society of Chemistry be held responsible for any errors or omissions in this *Accepted Manuscript* or any consequences arising from the use of any information it contains.

Graphical abstract for:

Preparation and properties of g-C₃N₄/AgBr nanocomposite photocatalyst based on protonation pretreatment

Protonation pretreatment promotes the formation of uniform g-C₃N₄/AgBr nanocomposite, thereby efficiently enhancing photocatalytic activity through the Z-scheme charge transfer.



ARTICLE

Preparation and properties of g-C₃N₄/AgBr nanocomposite photocatalyst based on protonation pretreatment

Cite this: DOI: 10.1039/x0xx00000x

Yu Feng,^a Jianchao Shen,^a Qifeng Cai,^a Hui Yang,^{a,b} and Qianhong Shen^{a,b*}

Received 00th January 2012,

Accepted 00th January 2012

DOI: 10.1039/x0xx00000x

www.rsc.org/

A novel method was proposed to fabricate g-C₃N₄/AgBr nanocomposite photocatalyst by loading AgBr nanoparticles on the g-C₃N₄ matrix, which was protonated under hydrothermal conditions in the presence of sulfuric acid. X-ray diffraction (XRD), Fourier transform infrared spectra (FT-IR), scanning electron microscopy (SEM), transmission electron microscopy (TEM), Brunauer-Emmett-Teller (BET), UV-vis diffuse reflectance spectra (DRS), electrochemical impedance spectroscopy (EIS), electron paramagnetic resonance (EPR), photoluminescence (PL) and reactive species trapping measurement were adopted to analyze the structure and properties of g-C₃N₄/AgBr nanocomposite photocatalyst. The photocatalytic activities of the as-prepared samples were also evaluated by decomposing methyl orange (MO) in aqueous solution under visible light illumination. The results show that the protonation pretreatment of g-C₃N₄ matrix can not only provide growth sites for AgBr grains, but also increase porosity of g-C₃N₄ matrix. Therefore, the AgBr nanoparticles can be uniformly loaded on the surface of g-C₃N₄ matrix, and the specific surface area of the composite can be increased obviously. As a result, the best photodegradation rate of MO over g-C₃N₄/AgBr nanocomposite photocatalyst is 33.8 and 2.1 times higher than that over pure g-C₃N₄ and AgBr samples, respectively. Combining the results of EIS Nyquist plots, EPR spectroscopy, reactive species trapping measurement and •OH trapping PL spectra, a Z-scheme charge transfer mechanism is proposed.

1. Introduction

With the increasing deterioration of the environment, semiconductor photocatalysis has attracted much research attention.^{1,2} Among various semiconductor materials, TiO₂ has been widely studied owing to its photochemical stability, nontoxicity, and low cost.³⁻⁶ However, only UV light, a small part (3-5%) of solar irradiation, can excite electrons in the valence band of TiO₂ due to its wide band gap (3.2 eV for anatase phase), thus obstructing its application in environmental protection field.⁵ Therefore, a new visible-light-driven photocatalyst has become a hot research topic.⁷⁻¹²

Recently, a polymeric semiconductor on the basis of a graphitic carbon nitride (g-C₃N₄) possessing an appropriate band gap (2.7 eV) and excellent chemical/thermal stability, has become a promising visible-light photocatalyst.^{13,14} The simple polymer semiconductor, consist of only carbon, nitrogen and some minor hydrogen content, is obviously "green".⁹ Furthermore, the g-C₃N₄ can be simply obtained by directly heating nitrogen-rich precursors such as cyanamide, dicyandiamide or melamine, and is regarded as the most stable phase among all the allotropes of carbon nitrides at ambient conditions.⁹ However, the g-C₃N₄ synthesized from the polycondensation of these precursors often result in a low specific surface area, thereby inhibiting its photocatalytic activity.^{8,15} Therefore, a rational treatment is necessary to enlarge its specific surface area.

In the present work, we report a new and novel method to modify g-C₃N₄ under hydrothermal conditions in the presence of sulfuric

acid by protonation effect. Owing to the protonation pretreatment, the specific surface area of g-C₃N₄ is increased, and the formed defects can introduce more active sites. These modifications in the structure of g-C₃N₄ are in favor of improving its adsorption capacity, photocatalytic ability and acting as a kind of matrix materials.

Silver bromide (AgBr) is a fascinating semiconductor with band gap of ~2.6 eV, which enables it to absorb sunlight up to 480 nm or even longer, and has been widely used as a photocatalyst material for the degradation of pollutants.^{16,17} The conduction band and the valence band of the AgBr are located at 0.06 eV and 2.55 eV, respectively,¹⁶ so it is very appropriate to combine it with g-C₃N₄ to form a heterojunction. This kind of composite system has also been studied by other researchers and proven to be an efficient way to modify g-C₃N₄.¹⁸⁻²⁰

On these bases, we fabricate a g-C₃N₄/AgBr nano-heterojunction photocatalyst by loading AgBr nanoparticles on the pretreated g-C₃N₄ matrix. Due to the introduced active sites by formed nanopores and defects under protonation pretreatment, the AgBr nanoparticles can in-situ grow on the pretreated g-C₃N₄ matrix to obtain a uniform nanocomposite photocatalyst. The visible light photocatalytic activities of the g-C₃N₄/AgBr heterojunctions are evaluated by using methyl orange (MO) as a target pollutant. The relationships between the photocatalytic activity and the structure of the heterojunction are also discussed. And a Z-scheme charge transfer is believed to be a likely mechanism for the enhancement of photocatalytic activities.

2. Experimental

The melamine was purchased from Aladdin Industrial Corporation, and other reagents were purchased from Sinopharm Chemical Reagent Co., Ltd. All the reagents for synthesis and analysis were analytical reagent grade and used without further treatment.

2.1 Preparation and protonation pretreatment of g-C₃N₄

The typical preparation method of g-C₃N₄ is as follows: 3 g of melamine powder was put into a corundum boat and heated to 653 K in 10 minutes and then heated to 793 K in a muffle furnace for 4 h at a heating rate of 2 K min⁻¹ in a flowing argon atmosphere prior to cooling. The resultant g-C₃N₄ (denoted as CN) was collected and milled into powder for further use.

The CN powder was protonated via hydrothermal method. Firstly, 500 mg CN powder was added into 50 ml of isopropanol, and the suspensi solution on was sonicated for 6 h. Next, the ultrasonic powder was directly dried at 353 K overnight. Secondly, the dried powder was added into 20 ml of ethanol and sonicated for 1 h, and then 20 ml of H₂SO₄ aqueous solution with concentration of 0.4 mol/L was added into the suspension. The mixture was stirred magnetically for 18 h and heated in water bath at 353 K for 4 h, and then was transferred to a Teflon-lined stainless steel autoclave of 50 ml capacity and maintained at 423 K for 20 h. After cooling to room temperature naturally, the precipitate was collected, washed with deionized water and absolute ethanol for three times, and then dried in air at 333 K to obtain modified g-C₃N₄ (denoted as MCN).

2.2 Preparation of g-C₃N₄/AgBr nanocomposite photocatalyst

In a typical experiment, 150 mg of MCN was added into 20 ml ethanol and sonicated for 1 h. Then, 50 ml of hexadecyl trimethyl ammonium bromide (CTAB) aqueous solution with a certain concentration was added into the suspension, and the mixture was stirred magnetically for 12 h. Next, AgNO₃ was dissolved in 50 ml aqueous solution, and was very slowly added to the above mixture. After completely added the AgNO₃ aqueous solution, the resulting suspension was stirred for 6 h. The final product was filtered and washed with deionized water and absolute ethanol for three times, and then dried at 333 K. According to this method, g-C₃N₄/AgBr composites with different amount of AgBr were prepared (denoted as MCN/AB-X, X is the mass percent of AgBr). The pure AgBr without adding MCN was also prepared by the same method.

For comparison, the raw g-C₃N₄ was used to prepare g-C₃N₄/AgBr by the same procedure (denoted as RCN/AB-X, X is the mass percent of AgBr).

2.3 Characterization

The crystal structure was characterized by an X-ray diffractometer (XRD, APEXII, Bruker, Germany) using Ni-filtered Cu K α radiation ($\lambda = 1.542 \text{ \AA}$). FT-IR spectra were recorded in transmission mode from 4000 to 400 cm⁻¹ on a FT-IR spectrometer (Avatar 360, Nicolet, USA) using the standard KBr disk method. Structure and morphology were investigated using field emission scanning electron microscopy (FE-SEM, SU-70, Hitachi, Japan) and transmission electron microscopy (TEM, TECNAI-10, Hitachi, Japan). The BET specific surface areas were measured by N₂ adsorption at 77 K on an adsorption analyzer (Quantachrome Ins, ASIC-2, USA). UV-vis diffuse reflectance spectra (DRS) were performed on a UV-vis spectrophotometer (UV-3150, Hitachi, Japan) using BaSO₄ as the reference. Absorption spectra were calculated from the reflectance data with the Kubelka-Munk function.

Electrochemical impedance spectroscopy (EIS) was measured on an electrochemical analyzer (CHI-760B, China) at 0 V (vs. SCE). A sinusoidal ac perturbation of 5 mV was applied to the electrode over the frequency range of 0.05–10⁵ Hz. The conventional three-electrode system was used. The prepared sample was served as a working electrode, while a Pt wire and a saturated calomel electrode (SCE) was employed as a counter electrode and a reference electrode respectively. Na₂SO₄ solution with concentration of 0.5 mol/L was used as electrolyte solution. A 300 W Xe lamp with a UV-cut off filter (> 420 nm) was served as a light source. The working electrode was prepared as follows: a fluorine-doped tin oxide (FTO) glass piece with a size of 1 cm \times 2 cm was cleaned by acetone, boiling NaOH (0.1 mol/L) and deionized water, respectively. 2 mg powder was mixed with 0.2 ml ethanol under sonication for 30 min to get slurry. Conductive adhesive with a size of 0.75 cm \times 0.75 cm was pressed on the bottom center of FTO glass. Finally, the as-prepared slurry was spreading onto the exposed electrically conductive adhesive and these electrolytes were dried at 80 °C for 2 h.¹⁵

Electron paramagnetic resonance (EPR) measurements were operated at a Bruker model A300 spectrometer with a 300 W Xe lamp equipped with an UV-cut off ($\lambda > 420 \text{ nm}$) as visible light source (microwave frequency: 9.857 GHz, microwave power: 20.20 mW, receiver gain: 1×10^4 , modulation frequency: 100 kHz, modulation amplitude: 3 G, Sweep time: 30.72 s). The calibration of the g values was performed using 2,2-diphenyl-1-picrylhydrazyl.

2.4 Photocatalysis evaluation

The photocatalytic activity of obtained samples were evaluated by degrading methyl orange (MO) in aqueous solution under visible light illumination. A 35 W CDM-T Philips metal halide lamp with a 420 nm UV-cut off filter was used as the visible light source. In each experiment, 50 mg of photocatalyst powder was suspended into 100 ml MO solution with a concentration of 10 mg/L. Prior to illumination, the suspension was magnetically stirred in the dark for 2 h to establish an adsorption-desorption equilibrium. The suspension is magnetically stirred throughout the process of photocatalytic reaction. When the reaction time is reached, approximately 4 ml of the suspension is centrifuged (9000 rpm, 8 min) to remove the photocatalyst from the solution. The resulting supernatant was analyzed using a UV-vis spectrophotometer (Lambda20, PerkinElmer, USA) and the characteristic absorption peak of MO at 464 nm was used to determine the extent of its decomposition.

2.5 Detection of reactive species

The detection of reactive oxidative species was similar to the photodegradation experimental process. A number of scavengers such as isopropanol (IPA) and benzoqui-none (BQ) were added into the MO solution prior to photocatalytic activity test. The concentration of IPA and BQ was 2.0 and 0.1 mmol/L in the MO solution (100 ml), respectively.^{21, 22} Further, hydroxyl radicals trapping photoluminescence (PL) experiment was used to detect the amount of $\cdot\text{OH}$ during the photocatalytic reactions.²³ The measurement was similar to photocatalytic test except the MO solution was replaced by aqueous solution. In a typical run, 50 mg of MCN/AB-60 was added to an aqueous solution, which contained 0.01 mol/L NaOH and 5×10^{-3} mol/L terephthalic acid (TA) in a 250 ml beaker. After reaching adsorption-desorption equilibrium, approximately 4 ml of mixture was collected in every 30 min during the illumination. Then the slurry sample was centrifuged (9000 rpm,

8 min) to remove the photocatalyst. The resulting supernatant was analyzed on a photoluminescence spectrometer (FLS920, Edinburgh, UK) using Xe lamp with excitation wavelength of 316 nm.

3. Results and discussion

MCN/AB nanocomposites were prepared by loading AgBr nanoparticles on the protonated $g\text{-C}_3\text{N}_4$ matrix. The protonation pretreatment of $g\text{-C}_3\text{N}_4$ can lead to the formation of defects and porous structure in $g\text{-C}_3\text{N}_4$. Therefore, the resulted MCN matrix can easily adsorb substances such as Br^- ions that generated from CTAB. And the AgBr nanoparticles tend to grow on the surface of MCN rather than in the solution after adding Ag^+ ions. Due to the existence of rich nanopores, the AgBr nanoparticles were localized and stabilized.

Fig. 1a shows the XRD patterns of the as-prepared samples. The CN sample displays a typical feature of $g\text{-C}_3\text{N}_4$ with two peaks at 27.4° and 13.2° , corresponding to the (002) and (100) diffraction planes which represent the interplanar peak of aromatic systems and planar structural packing motif (JCPDS 87-1526) respectively.²⁴ After treating CN under hydrothermal conditions in the presence of sulfuric acid, the XRD pattern of the obtained MCN shows the characteristic peak at 27.4° , whereas the low angle diffraction peak at 13.2° becomes weak, suggesting that the typical layered structure of $g\text{-C}_3\text{N}_4$ is well kept, while the orderliness of planar structure decreases after the intense protonation.^{24,25} Furthermore, the diffraction peaks corresponding to the phase of AgBr (JCPDS 6-438) are observed in the MCN/AB nanocomposite photocatalyst. This indicates that the nanocomposite photocatalysts contain two crystal phases of AgBr and $g\text{-C}_3\text{N}_4$.

Functional groups of the samples are confirmed by FT-IR spectra. As shown in Fig. 1b, CN and MCN have the similar FT-IR spectrum. The strong bands in the $1200\text{-}1650\text{ cm}^{-1}$ region correspond to the typical stretching vibration modes of C-N and C=N heterocycles.⁸ Additionally, the characteristic breathing mode of the triazine units at 807 cm^{-1} and the broad bands at around 3200 cm^{-1} , which indicates of N-H stretching vibration modes, are also observed.^{8,9} It should be noted that a new band appears at 620 cm^{-1} in MCN. This may be contributed to the SO_4^{2-} that adsorbed in the surface of MCN.²⁶ All the MCN/AB photocatalysts show similar spectra due to the strong IR response of MCN.

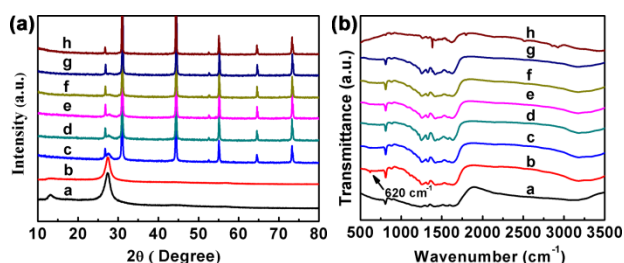


Fig. 1 (a) XRD patterns and (b) FT-IR spectra of **a** CN, **b** MCN, **c** MCN/AB-30, **d** MCN/AB-50, **e** MCN/AB-60, **f** MCN/AB-70, **g** MCN/AB-80 and **h** AgBr.

Fig. 2 shows the SEM images of as-prepared samples. The CN sample exhibits a plate-like structure. However, after hydrothermal treatment in the presence of sulfuric acid, the CN may decompose to clusters/oligomers of condensed triazine-rings, some of which with good water-solubility will be removed by decomposition under hydrothermal conditions, leading to the formation of porous network structures in layered $g\text{-C}_3\text{N}_4$ (Fig. 2b), and the specific surface area is therefore enlarged from $3.5\text{ m}^2\text{g}^{-1}$ to $40.0\text{ m}^2\text{g}^{-1}$ (Fig. S1, ESI†). Moreover, the protonation effect may also increase the defects on the

surface of $g\text{-C}_3\text{N}_4$, thereby providing growth sites for AgBr grains.^{24,25} As a result, AgBr nanoparticles can be loaded on $g\text{-C}_3\text{N}_4$ more uniformly (Fig. 2c-f). In addition, the particle size of pure AgBr particles is extremely increased to a large value ($\sim 1\text{ }\mu\text{m}$) in the absence of MCN (Fig. 2h). This suggests that the rich nanopores and defects in MCN could serve as the AgBr nucleation sites.²⁰ For comparison, the raw $g\text{-C}_3\text{N}_4$ was also used to prepare $g\text{-C}_3\text{N}_4/\text{AgBr}$ nanocomposite (RCN/AB-60). It can be seen from the Fig. S2a (ESI†) that AgBr particles mainly disperse in the medium and aggregate together, rather than deposit on the surface of CN matrix and the particle size ($0.8\text{-}1\text{ }\mu\text{m}$) is much larger than that of the MCN/AB. It seems that the protonation pretreatment of $g\text{-C}_3\text{N}_4$ matrix plays an important role in promoting such heterogeneous growth. The TEM image of MCN/AB-60 in Fig. S2b (ESI†) clearly shows that the individual AgBr nanoparticles ($\sim 100\text{ nm}$) are uniformly deposited on the porous surface of MCN. And the interaction between the AgBr nanoparticles and the MCN matrix may be relatively strong, particularly considering a long time ultrasonication (30 min) during the sample preparation procedure for TEM analysis.

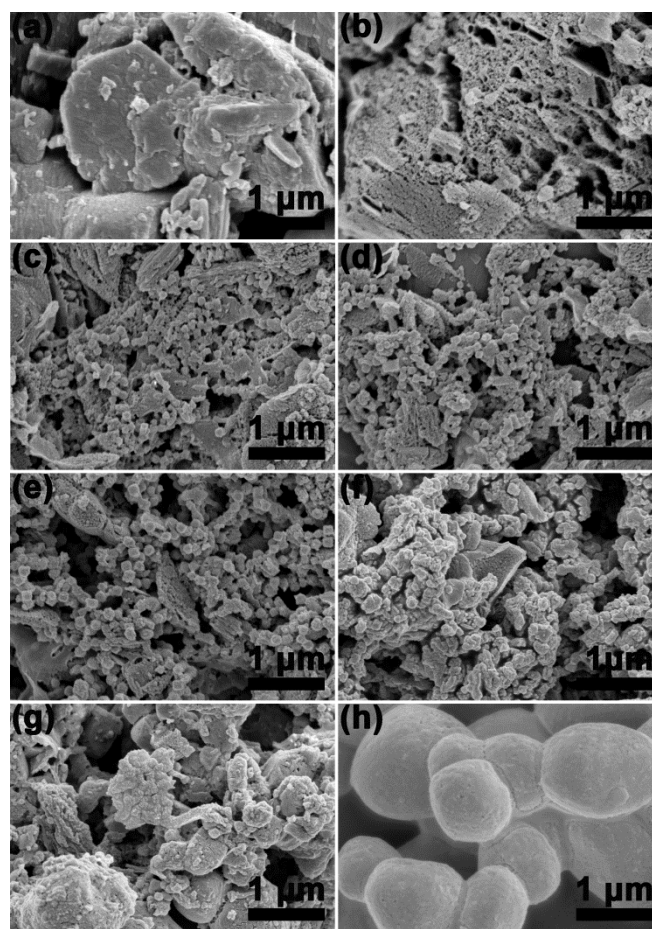


Fig. 2 SEM images of (a) CN, (b) MCN, (c) MCN/AB-30, (d) MCN/AB-50, (e) MCN/AB-60, (f) MCN/AB-70, (g) MCN/AB-80 and (h) AgBr.

Fig. 3 shows UV-vis diffuse reflectance spectra of as-prepared samples. The band edge wavelength of $g\text{-C}_3\text{N}_4$ is blue-shifted from 463 nm to 446 nm after the protonation pretreatment. The protonation induces the formation of porous $g\text{-C}_3\text{N}_4$ as well as the refinement of $g\text{-C}_3\text{N}_4$ particles. Therefore, the blue-shift of band edge wavelength is probably due to the quantum confinement

effect.²⁷ After combining MCN with AgBr, the absorption edges are located in 446 nm (MCN)-495 nm (AgBr) regions, which is contributed to the optical response of AgBr and MCN as well as the combination of these two semiconductors.^{24,28} Furthermore, it can be seen from the plot of $(\alpha h\nu)^{1/2}$ versus photon energy that the band gap of MCN/AB samples is decreased from 2.78 eV to 2.51 eV with increasing the content of AgBr.

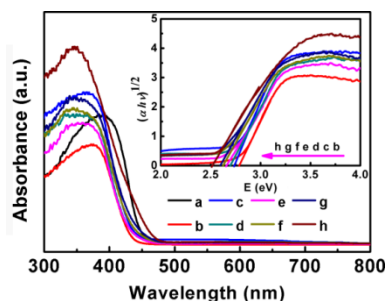


Fig. 3 UV-vis DRS of **a** CN, **b** MCN, **c** MCN/AB-30, **d** MCN/AB-50, **e** MCN/AB-60, **f** MCN/AB-70, **g** MCN/AB-80 and **h** AgBr. The inset shows the corresponding band gap of as-prepared samples.

The photocatalytic activities of all the samples are evaluated by methyl orange (MO) photocatalytic degradation under visible light ($\lambda > 420$ nm) illumination. As shown in Fig. 4a, the absorbance of MO solution displays little change during the visible light illumination for 2 h, indicating that MO is quite stable under the illumination of this light source. The CN shows a low photocatalytic activity. After the protonation pretreatment, the photocatalytic activity of **i** is improved to some degree, the decomposition ratio of MO reaches 29.7%. However, when combining MCN with AgBr, the photocatalytic activity is significantly enhanced and increased with the content of AgBr. The highest activity is obtained for the MCN/AB-60 sample, over which about 78.9% of MO can be degraded. In addition, although the activity is decreased when further increasing the AgBr content, it is still higher than that of AgBr or MCN. Note that the degradation rate of MO over RCN/AB-60 is about 65.1%, and is lower than that of MCN/AB-60. This was mainly due to the uniform distribution of AgBr, more contact area of heterojunction and more active points in MCN/AB-60.

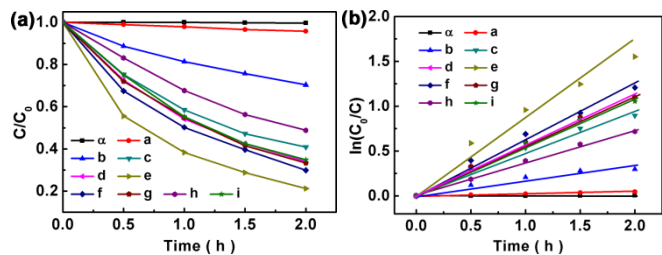


Fig. 4 (a) Photocatalytic activities and (b) the photocatalytic degradation kinetics of **a** MO photolysis, **a** CN, **b** MCN, **c** MCN/AB-30, **d** MCN/AB-50, **e** MCN/AB-60, **f** MCN/AB-70, **g** MCN/AB-80, **h** AgBr and **i** RCN/AB-60 for MO degradation under visible-light illumination.

The photocatalytic decomposition kinetics of the as-prepared sample is fitted by a pseudo-first-order model, which is depicted by the equation:

$$\ln(C_0/C_t) = kt$$

where C_0 and C_t are the MO concentrations in solution at times 0 and t respectively, and k is the apparent first-order rate constant. As

shown in Fig. 4b, the MCN/AB-60 nanocomposite photocatalyst exhibits the highest photocatalytic decomposition rate of 0.75 h^{-1} , which is 33.8, 5.0, 2.1 and 1.4 times higher than that of CN, MCN, AgBr and RCN/AB-60, respectively. The first-order rate constant is not proportional to the mass ratio of MCN/AB, which suggests that the combination of MCN and AgBr may form an efficient junction and lead to some positive synergy.

For practical applications, the reusability of photocatalysts should be considered. The reusability of the MCN/AB-60 was further investigated by recycling the photocatalyst for MO degradation under visible light irradiation. As shown in Fig. 5, about 68.5% of MO dyes can be degraded in the second time, which was lower than the first time (78.9%). However, no apparent decrease of photocatalytic activity is observed in the following recycling. This phenomenon was also observed in other's work and may be related to the reduced AgBr during the first and second photocatalytic process.²⁹ More importantly, the photocatalytic ability is still well-kept at a high level in the 4th time of photocatalytic behaviour.

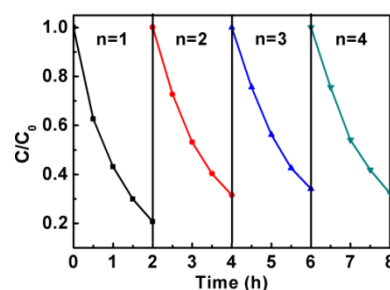


Fig. 5 Photostability experiments of MCN/AB-60 photocatalyst for MO degradation under visible-light illumination.

Generally, phase structure, adsorption ability, separation efficiency of photo-generated carriers are crucial factors of photocatalytic activity.^{11,30} Based on the above analysis, it can be seen that the typical layered structure of $g\text{-C}_3\text{N}_4$, as well as melem structure served as a visible-light sensitizer, is well kept after the intense protonation. Moreover, the obtained MCN/AB composite samples contain two fundamental components of $g\text{-C}_3\text{N}_4$ and AgBr with well-matched band structure, which is favorable for the highly efficient interparticle electron transfer. The morphology of the MCN/AB composites determines the adsorption ability and separation efficiency of photo-generated carriers. The protonation pretreatment can increase porosity of $g\text{-C}_3\text{N}_4$, resulting in high adsorption ability for contaminant molecules (Fig. S3, ESI†). In addition, the intense protonation can also provide growth sites for AgBr grains, thereby obtaining a uniform composite morphology as well as a high efficient nanojunction structure.

The separation efficiency of photo-generated electrons and holes plays an important role in enhancing photocatalytic activity.¹¹ The interface charge separation efficiency can be investigated by EIS. Fig. 6 shows the EIS Nyquist plots of different samples with or without visible light illumination. A smaller arc radius of the EIS Nyquist plot reflects a higher efficient charge transfer occurring at the interface.¹¹ Therefore, the MCN/AB-60 exhibits a more effective separation of photo-generated charge carriers due to its smallest arc radius. These results indicate that the introduction of AgBr can form MCN/AB nanojunction, and thus dramatically enhance the separation and transfer efficiency of photo-generated electron-hole pairs.

The in-situ EPR spectroscopy is used to detect conduction band electrons during the illumination.^{31,32} A g value of 2.0035 is measured for the single Lorentzian lines of all the samples even before the illumination (Fig. 7a, black curve), which can be

attributed to an unpaired electron on the carbon atoms of the aromatic rings within π -bonded nanosized clusters.³³⁻³⁵ The EPR signal (Fig. 7a, black curve) of MCN or MCN/AB-60 is higher than that of CN due to their higher surface areas.³⁶ Moreover, EPR signals of all the samples during (Fig. 7a, red curve) and after (Fig. 7a, gray curve) illumination were also detected and further double integrated to analyse the process of charge transfer more clearly (Fig. 7b). For the CN sample, a signal of conduction band electrons is obtained during illumination (dark full dot) and then vanishes after switching off the light (dark empty dot), indicating a fast recombination of carriers in the CN sample. In contrast, the EPR signal of MCN/AB-60 exhibits the smallest decrease after the illumination. These results suggest that the recombination of carriers is efficiently inhibited in this nanocomposite system.

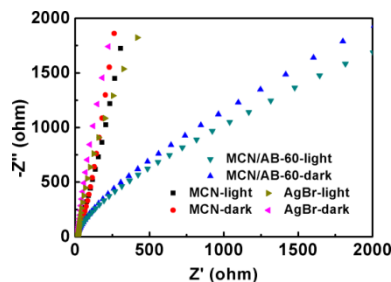


Fig. 6 EIS Nyquist plots for the MCN, AgBr and MCN/AB-60.

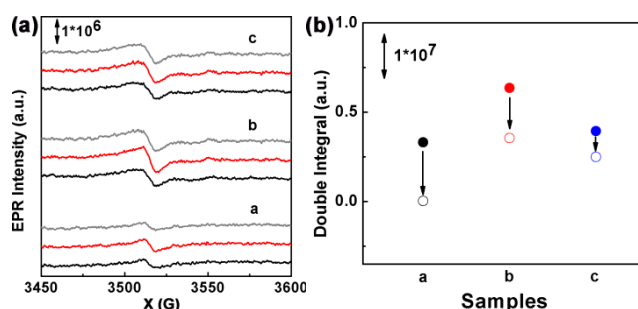


Fig. 7 (a) EPR signals (before illumination-black, during illumination-red, after illumination-gray) and (b) double integral of the EPR signal of a CN, b MCN and c MCN/AB-60 (during illumination-full dot, after illumination-empty dot).

To reveal the photocatalytic mechanism, isopropanol (IPA, \bullet OH quencher), benzoquinone (BQ, \bullet O₂⁻¹ quencher) are adopted to find which reactive species plays the primary role for MO degradation over MCN/AB-60 photocatalyst. It can be seen from Fig. 8a that the degradation of MO is inhibited significantly after the addition of BQ, whereas there are only small changes in the degradation of MO when adding IPA. Furthermore, terephthalic acid (TA) is used to detect the formation of \bullet OH in the reaction system under visible-light illumination and the results are shown in Fig. 8b. The PL signal at 425 nm is observed and gradually increased during the illumination, indicating that the \bullet OH is generated and increased with the illumination.³⁷ The results suggest that the main reactive species generated from MCN/AB-60 reaction system is \bullet O₂⁻¹ rather than \bullet OH although \bullet OH is generated in the system.

On the basis of the above results, a Z-scheme charge transfer mechanism is proposed.^{38,39} The Mulliken electronegativity theory can be used to calculate the potentials of the conduction band (CB) and valence band edge (VB) of MCN and AgBr. The theory is depicted by the following equation.^{18,39}

$$E_{CB} = X - E_C - \frac{1}{2}E_g$$

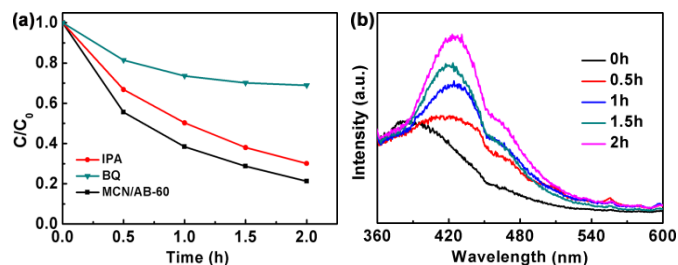


Fig. 8 (a) Effects of IPA and BQ on the MO degradation over MCN/AB-60. (b) \bullet OH trapping PL spectra of MCN/AB-60 in TA solution under visible-light illumination.

where X is the absolute electronegativity of the atom semiconductor; E_C is the energy of free electrons with the hydrogen scale; E_g is the band gap of the semiconductor. Therefore, the CB and VB edge potentials of MCN can be determined about -1.17 eV and 1.61 eV respectively, while the CB and VB edge potentials of AgBr are about 0.05 eV and 2.56 eV respectively. These results are similar with the previous reports.^{16,18} When these two semiconductors combined together, the appropriate energy level will impel them to form a heterojunction. The likely photocatalysis mechanism is proposed in Fig. 9. In the photocatalytic process, the nanocomposite photocatalyst is excited by visible light, both the MCN and AgBr can absorb photons and yield electrons and holes. According to the traditional charge-carrier transfer mechanism, the photo-generated electrons in the CB of MCN will migrate to the CB of AgBr, and photo-generated holes in the VB of AgBr will migrate to the VB of MCN. However, these accumulated electrons in the CB of AgBr ($E_{CB} = 0.05$ eV) can not reduce O₂ to yield \bullet O₂⁻¹ ($E^0(\text{O}_2/\bullet\text{O}_2^{-1}) = -0.33$ eV/NHE),²¹ and the holes in the VB of MCN ($E_{VB} = 1.61$ eV) can not oxidize H₂O to give \bullet OH ($E^0(\bullet\text{OH}/\text{H}_2\text{O}) = 2.27$ eV/NHE).⁴⁰ As a result, this mechanism is inconsistent with the fact here that the \bullet O₂⁻¹ is a main reactive species. Therefore, a Z-scheme charge transfer mechanism is proposed to explain the experimental phenomena. It is believed that a fast recombination may occur between the photo-generated electrons in the CB of AgBr and photo-generated holes in the VB of MCN. Meanwhile, the electrons in the CB of MCN ($E_{CB} = -1.17$ eV), which have more negative potentials, can efficiently reduce O₂ to yield \bullet O₂⁻¹ radicals. Whereas the holes in the VB of AgBr ($E_{VB} = 2.56$ eV) have more positive potentials, and thus can generate more active \bullet OH radicals. This Z-scheme charge transfer mechanism is also consistent with the EPR result, that MCN/AB-60 has a smaller EPR signal than MCN during the illumination. Consequently, a typical Z-scheme nano-heterojunction is built between MCN and AgBr.

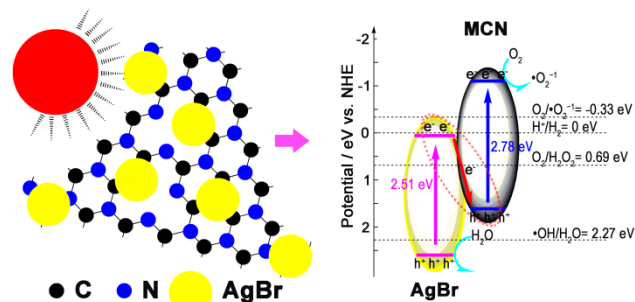


Fig. 9 Scheme for electron-hole pairs separation and the Z-scheme charge transfer mechanism over MCN/AB photocatalyst under visible-light illumination.

4. Conclusions

In summary, a highly efficient g-C₃N₄/AgBr nanocomposite photocatalyst was prepared by loading AgBr nanoparticles on the protonated g-C₃N₄ matrix. The protonation pretreatment can efficiently increase the specific surface area of g-C₃N₄, and the formed defects can introduce more active sites, promoting the in-situ growth of AgBr nanoparticles on g-C₃N₄ matrix. Thereby, the g-C₃N₄/AgBr nanocomposite obtains a relatively uniform composite morphology. The efficient combination of g-C₃N₄ and AgBr leads to Z-scheme charge transfer in the composite system, and the photocatalytic activity is therefore enhanced significantly. The protonation pretreatment method is expected to be expanded for the preparation of other g-C₃N₄ based composite materials.

Acknowledgements

We would like to thank Key Technologies R&D Program of China under Grant No.2013BAJ10B05, Fundamental Research Funds for the Central Universities under Grant No.ZJUR011104.

Notes and references

^a State Key Laboratory of Silicon Materials, Department of Materials Science & Engineering, Zhejiang University, Hangzhou 310027, P. R. China. E-mail: s_qianhong@163.com; Fax: +86 571 87953313; Tel: +86 0571 87953313.

^b Zhejiang California International NanoSystems Institute, Zhejiang University, Hangzhou 310027, P. R. China.

† Electronic Supplementary Information (ESI) available: See DOI: 10.1039/c000000x/

- R. Asahi, T. Morikawa, T. Ohwaki, K. Aoki and Y. Taga, *science*, 2001, **293**, 269-271.
- T. Ohno, K. Sarukawa and M. Matsumura, *New Journal of Chemistry*, 2002, **26**, 1167-1170.
- Y. Liang, H. Wang, H. S. Casalongue, Z. Chen and H. Dai, *Nano Research*, 2010, **3**, 701-705.
- Y. J. Kim, B. Gao, S. Y. Han, M. H. Jung, A. K. Chakraborty, T. Ko, C. Lee and W. I. Lee, *The Journal of Physical Chemistry C*, 2009, **113**, 19179-19184.
- X. Chen and S. S. Mao, *Chem Rev*, 2007, **107**, 2891-2959.
- J. G. Yu, J. C. Yu, W. K. Ho and Z. T. Jiang, *New Journal of Chemistry*, 2002, **26**, 607-613.
- W.-C. Huang, L.-M. Lyu, Y.-C. Yang and M. H. Huang, *Journal of the American Chemical Society*, 2011, **134**, 1261-1267.
- J. Fu, B. Chang, Y. Tian, F. Xi and X. Dong, *Journal of Materials Chemistry A*, 2013, **1**, 3083-3090.
- S. Yan, Z. Li and Z. Zou, *Langmuir*, 2009, **25**, 10397-10401.
- J. Di, J. Xia, S. Yin, H. Xu, M. He, H. Li, L. Xu and Y. Jiang, *RSC Adv.*, 2013, **3**, 19624-19631.
- Y. Wang, X. Bai, C. Pan, J. He and Y. Zhu, *Journal of Materials Chemistry*, 2012, **22**, 11568-11573.
- Y. X. Zhou, L. Tong, X. H. Zeng and X. B. Chen, *New Journal of Chemistry*, 2014, **38**, 1973-1979.
- X.-H. Li, X. Wang and M. Antonietti, *Chem. Sci.*, 2012, **3**, 2170-2174.
- C. Han, L. Ge, C. Chen, Y. Li, X. Xiao, Y. Zhang and L. Guo, *Applied Catalysis B: Environmental*, 2014, **147**, 546-553.
- Y. He, J. Cai, T. Li, Y. Wu, Y. Yi, M. Luo and L. Zhao, *Industrial & Engineering Chemistry Research*, 2012, **51**, 14729-14737.
- J. Cao, B. Luo, H. Lin, B. Xu and S. Chen, *Journal of hazardous materials*, 2012, **217**, 107-115.
- W. Wang, L. Jing, Y. Qu, Y. Luan, H. Fu and Y. Xiao, *Journal of hazardous materials*, 2012, **243**, 169-178.
- H. Xu, J. Yan, Y. Xu, Y. Song, H. Li, J. Xia, C. Huang and H. Wan, *Applied Catalysis B: Environmental*, 2013, **129**, 182-193.
- Y. G. Xu, H. Xu, J. Yan, H. M. Li, L. Y. Huang, J. X. Xia, S. Yin and H. M. Shu, *Colloids and Surfaces a-Physicochemical and Engineering Aspects*, 2013, **436**, 474-483.
- Y. H. Lan, X. Z. Qian, C. J. Zhao, Z. M. Zhang, X. Chen and Z. Li, *J Colloid Interface Sci*, 2013, **395**, 75-80.
- S. Wang, D. Li, C. Sun, S. Yang, Y. Guan and H. He, *Applied catalysis. B, Environmental*, 2014, **144**, 885-892.
- S. Kumar, T. Surendar, A. Baruah and V. Shanker, *Journal of Materials Chemistry A*, 2013, **1**, 5333-5340.
- Y. He, J. Cai, T. Li, Y. Wu, H. Lin, L. Zhao and M. Luo, *Chemical Engineering Journal*, 2013, **215**, 721-730.
- J. Shen, H. Yang, Q. Shen, Y. Feng and Q. Cai, *CrystEngComm*, 2014, **16**, 1868-1872.
- Y. Zhang, A. Thomas, M. Antonietti and X. Wang, *Journal of the American Chemical Society*, 2008, **131**, 50-51.
- D. Marinova, M. Georgiev and D. Stoilova, *J Mol Struct*, 2009, **929**, 67-72.
- B. Balamurugan, I. Aruna, B. Mehta and S. Shivaprasad, *Physical Review B*, 2004, **69**, 165419.
- J. Cao, Y. Zhao, H. Lin, B. Xu and S. Chen, *Materials Research Bulletin*, 2013, **48**, 3873-3880.
- J. Cao, Y. J. Zhao, H. L. Lin, B. Y. Xu and S. F. Chen, *Materials Research Bulletin*, 2013, **48**, 3873-3880.
- X. Bai, L. Wang and Y. Zhu, *ACS Catalysis*, 2012, **2**, 2769-2778.
- D. Hollmann, M. Karnahl, S. Tschierlei, K. Kailasam, M. Schneider, J. Radnik, K. Grabow, U. Bentrup, H. Junge, M. Beller, S. Lochbrunner, A. Thomas and A. Bruckner, *Chemistry of Materials*, 2014, **26**, 1727-1733.
- E. Dmitrieva and L. Dunsch, *The Journal of Physical Chemistry B*, 2011, **115**, 6401-6411.
- M. Tabbal, T. Christidis, S. Isber, P. Merel, M. El Khakani, M. Chaker, A. Amassian and L. Martinu, *Journal of applied physics*, 2005, **98**, 044310.
- D. Rovnyak, M. Baldus, B. A. Itin, M. Bennati, A. Stevens and R. G. Griffin, *The Journal of Physical Chemistry B*, 2000, **104**, 9817-9822.
- X. Wang, K. Maeda, A. Thomas, K. Takanabe, G. Xin, J. M. Carlsson, K. Domen and M. Antonietti, *Nature Mater*, 2008, **8**, 76-80.
- G. Zhang, J. Zhang, M. Zhang and X. Wang, *Journal of Materials Chemistry*, 2012, **22**, 8083-8091.
- N. Zhang, S. Liu, X. Fu and Y.-J. Xu, *The Journal of Physical Chemistry C*, 2011, **115**, 9136-9145.
- Z. Jin, N. Murakami, T. Tsubota and T. Ohno, *Applied Catalysis B: Environmental*, 2014, **150**, 479-485.
- S. Chen, Y. Hu, S. Meng and X. Fu, *Applied Catalysis B: Environmental*, 2014, **150-151**, 564-573.
- S. B. Rawal, S. Bera, D. Lee, D.-J. Jang and W. I. Lee, *Catalysis Science & Technology*, 2013, **3**, 1822-1830.